An Experimental Study of the Dynamics and Temporal Evolution of Self-Trapped Laser Beams in a Photopolymerizable Organosiloxane

ARTICLE *in* THE JOURNAL OF PHYSICAL CHEMISTRY C · OCTOBER 2008

Impact Factor: 4.77 · DOI: 10.1021/jp801342n

2 AUTHORS, INCLUDING:

Ana B. Villafranca
McMaster University
12 PUBLICATIONS **84** CITATIONS

SEE PROFILE

THE JOURNAL OF PHYSICAL CHEMISTRY C

Article

An Experimental Study of the Dynamics and Temporal Evolution of Self-Trapped Laser Beams in a Photopolymerizable Organosiloxane

Ana B. Villafranca, and Kalaichelvi Saravanamuttu

J. Phys. Chem. C, **2008**, 112 (44), 17388-17396 • DOI: 10.1021/jp801342n • Publication Date (Web): 10 October 2008

An Experimental Study of the Dynamics and Temporal Evolution of Self-Trapped Laser Beams in a Photopolymerizable Organosiloxane

Ana B. Villafranca and Kalaichelvi Saravanamuttu*

Department of Chemistry and Department of Engineering Physics, McMaster University, 1280 Main Street West, Hamilton, Ontario L8S 4M1, Canada

Received: September 18, 2007; Revised Manuscript Received: August 2, 2008

Self-trapping of a visible, continuous wave laser beam in a photopolymerizable organosiloxane was studied at intensities ranging across 10 orders of magnitude (3.2×10^{-5} to 12 732 W·cm^{-2}). The process was characterized in detail through spatial intensity profiles of the beam, temporal monitoring of its width and peak intensity combined with optical microscopy of the resulting self-written waveguides. These observations revealed a rich diversity of dynamic phenomena during the self-trapping process in different intensity regimes, including (i) complementary oscillations in width and peak intensity of self-trapped beams, (ii) *in situ* sequential excitation of high-order modes (corresponding to optical fiber modes) in self-written cylindrical waveguides, (iii) variations in modal composition during the transition of self-written waveguides from single to multimode guidance, (iv) generation of spatial diffraction rings, and (v) beam filamentation. Quantitative analyses of parameters such as self-focusing time, self-trapped beam width and light transmittance gave new insight into details of the self-trapping mechanism, particularly the significance of the spatial profile (gradient) of refractive index changes induced in the medium. The results of this comprehensive experimental study provide a deep understanding of the dynamics of self-trapping in a photopolymerizable medium, including the general process of waveguide self-writing, and are consistent with some predictions of earlier theoretical models, the most significant being the rare opportunity to individually observe high-order optical modes during the evolution of the waveguide. In addition, entirely new features such as the emergence of spatial diffraction rings require further theoretical and experimental investigations.

1. Introduction

The natural diffraction of light can be suppressed in a medium that exhibits photoinduced changes in refractive index. Under these conditions, a typically Gaussian beam becomes entrapped within a self-induced waveguide and propagates without broadening over distances much greater than the Rayleigh range. Self-trapped beams are expressed as solutions of the nonlinear Schrödinger equation, which describes competition between the natural diffraction and self-induced refraction of the beam.[1] Optical self-trapping has been studied across forty years[1] in materials as varied as Kerr media,[2] photorefractive crystals,[3] photosensitive glasses,[4] and photopolymerizable resins.[5−9] The dynamics and temporal evolution of self-trapped beams, however, are determined by the molecular origins of refractive index changes in the medium.[1,10a,b] Striking differences exist, for example, between self-trapping dynamics in the two most frequently employed materials, Kerr media and photorefractive crystals. Because refractive index changes in the former originate from the third-order susceptibility tensor, self-trapping can only be elicited with intense (GW·cm^{-2} to TW·cm^{-2}), short (10^{-15} s) pulses of light. The nonsaturable nature of the Kerr response moreover renders two-dimensional (2-D) self-trapped beams unstable, restricting experiments to planar waveguide (one-dimensional, or 1-D) configurations. While early studies of 1-D self-trapping in Kerr media were seminal and provided elegant mathematical solutions,[2] more recent research examined self-trapping in photorefractive crystals. Here, refractive index changes, which typically originate from the electro-optic effect, are saturable.[3,10] This facilitates 1-D and 2-D self-trapping at relatively small intensities; entirely new forms of self-trapped light,[3,10] including dark,[11,12] spatially incoherent,[13,14] and even white light solitons, have been discovered in photorefractive crystals.[15]

The research presented in this article examines the process of self-trapping in an organosiloxane medium, in which refractive index changes originate from a photoinitiated free-radical polymerization reaction.[16] This photochemical approach provides opportunities to examine the dynamics and temporal evolution of self-trapped beams, which are *entirely different* from self-trapping dynamics in nonlinear optical (Kerr, photorefractive) materials. This is because of the following fundamental differences in the photoresponse between them: (i) Index changes in Kerr media decay immediately upon removal of the light field and in photorefractive crystals, at timescales determined by the dielectric relaxation time of the medium; polymerization-induced refractive index changes are permanent and moreover, greater by at least an order of magnitude.[16] (ii) Polymerization can be initiated with a small amount of light-absorbing photoinitiator molecules; beam attenuation is therefore negligible. Depending on the wavelength and quantum yield of photoinitiation,[17] self-trapping in photopolymers can, in principle, be achieved at a large range of wavelengths and at extremely low optical intensities (μW·cm^{-2}). Refractive index changes in Kerr media by contrast must be induced at intensities of gigawatts per square centimeter. (iii) The photoresponse time in a polymerizable medium relies on photochemical reactions (ranging from ms to min), while, in Kerr media, it is determined by a virtually instantaneous electronic response (10^{-15} s), and in photorefractive media, it depends on the dielectric relaxation times, which can vary from nanoseconds to minutes.

* Corresponding author. E-mail: kalai@mcmaster.ca.

10.1021/jp801342n CCC: $40.75
Published on Web 10/10/2008

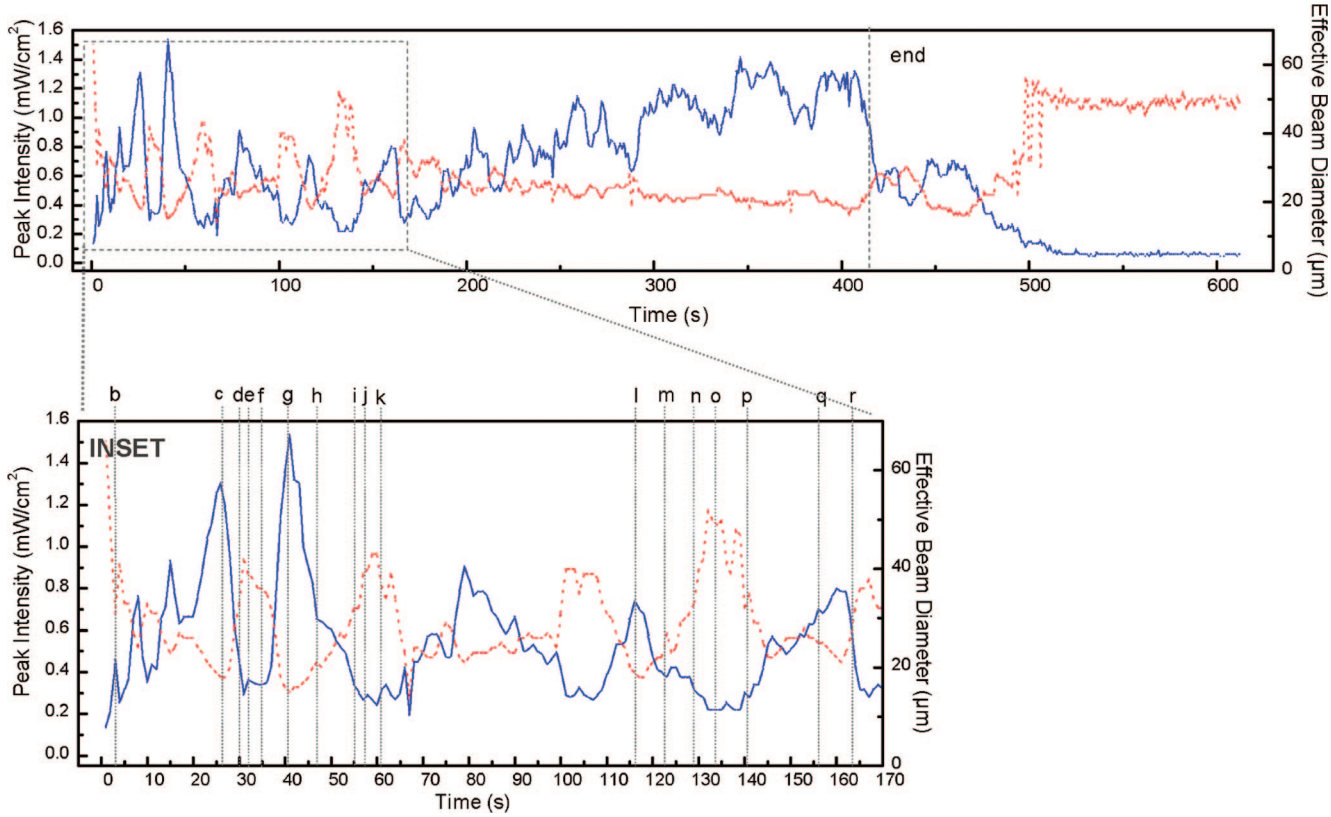

Figure 1. Temporal plots of peak intensity (solid blue line) and effective diameter (dotted red line) during self-trapping of a Gaussian visible (532 nm) laser beam at 1.6×10^{-2} W·cm^{-2} in the organosiloxane medium. Termination of self-trapping is indicated by the vertical dotted line at 415 s. The inset contains the time-period (0−170 s) corresponding to the onset of higher order modes. Times corresponding to 2-D spatial intensity profiles of the beam (Figure 2b−r) are marked by dotted lines.

Theoretical models based on the nonlinear Schrödinger equation have predicted several properties and trends in the behavior of self-trapped beams in polymerizable media.[5,6,18−22] These include the formation of multimode waveguides during self-trapping, the sequential excitation of high-order optical modes, and the complex evolution of the modal composition of the self-induced waveguide as it evolves from single-mode to multimode guidance. However, previous experimental studies of self-trapping in polymerizable media have been mainly concerned with channel waveguides induced by self-trapped beams, including tapered waveguides in epoxy resins[23] and cylindrical fibers in diacrylate and urethane−acrylate resins.[24] Related studies have also examined beam filamentation at increasing intensities,[9,24,25] interactions of self-trapped beams,[7,24] and spectroscopic monitoring of waveguide-formation.[26] Potential applications of waveguides as single-mode,[27] multimode[28] interconnects, fiber interconnects,[29,30] and components of wavelength division multiplexers[31,32] have been examined. Complex self-written structures including replicas of high-order modes on fiber-tips,[33] waveguide arrays,[34a,b] and even artificial compound eyes have also been demonstrated.[35a,b]

Collectively, the investigations listed above demonstrated that both 1-D[26] and 2-D[5−9] self-trapping could be achieved in polymerization systems and highlighted potential applications of self-written structures. By contrast, the study presented in this article intends to systematically determine the temporal evolution of self-trapped beams and quantitatively characterize their dynamics over a broad range of intensities across 10 orders of magnitude (3.2×10^{-5} to 12 732 W·cm^{-2}), and compare these observations with existing theoretical predictions. Two significant features set this study apart: (i) while previous experiments characterized self-trapping through the structure and properties of self-induced waveguides or light scattered along the beam path, we employed beam profiling methods to directly visualize and quantitatively measure changes in the cross-sectional intensity profiles of the beam; and (ii) the excellent spatial resolution in the photoresponse of the organosiloxane (∼ 150 nm)[36] enabled quantitative experiments over a broad range of intensities without blurring, a diffusion-caused problem that has hampered previous studies based on liquid monomers.[5,9]

Discussions of results are presented as follow. Detailed analysis of the observation of high-order modes during self-trapping at a single intensity 1.6×10^{-2} W·cm^{-2} is first presented in Section 2.1. Trends elucidated from the intensity-dependence of self-trapping observed at the entire range of intensities examined are then presented in Section 2.2.

2. Results and Discussion

2.1. Self-Trapping Dynamics: High-Order Modes.

2.1.1. Experimental Verification. In a typical experiment, a linearly polarized, Gaussian laser beam at 532 nm with an average intensity of 1.6×10^{-2} W·cm^{-2} was focused onto the entrance face of a transparent cuvette containing the photopolymerizable organosiloxane medium. Under linear conditions, the beam diffracted in both transverse directions from a focal width ($1/e^2$) of 20 to 118 μm (Figure 2a) as it propagated 6.0 mm from the entrance to the exit face of the medium. By contrast, in an organosiloxane sensitized to visible wavelengths with a titanocene photoinitiator (λ_{max} = 393 nm, 460 nm), the beam self-trapped and propagated without diffracting by initiating free-radical polymerization of methacrylate groups and corresponding refractive index changes (Δn). The organosiloxane, which has a refractive index of 1.47, undergoes a maximum change in refractive index of $\Delta n_s \sim 0.006$[16,45] (This value of

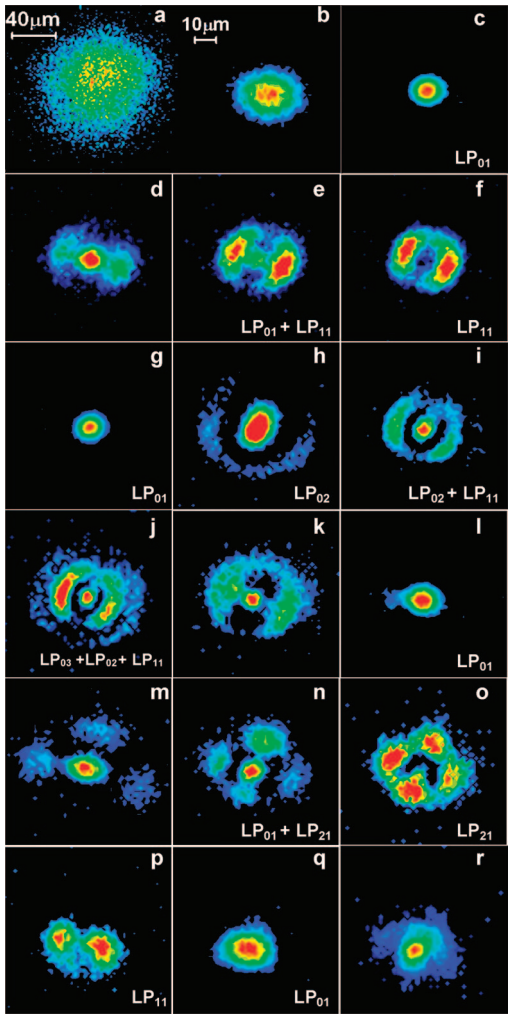

Figure 2. Temporal variations of 2-D spatial intensity profiles of the beam at the exit face (z = 6.00 mm) during self-trapping in the organosiloxane at 1.6 × 10^{-2} W·cm^{-2}. Profiles were acquired at (b) 3 s, (c) 27 s, (d) 30 s, (e) 32 s, (f) 35 s, (g) 41 s, (h) 47 s, (i) 55 s, (j) 57 s, (k) 61 s, (l) 116 s, (m) 123 s, (n) 129 s, (o) 134 s, (p) 141 s, (q) 156 s, and (r) 163 s. The 2-D profile of the beam acquired under linear conditions (a) is included for comparison. Mode labels follow standard optical fiber nomenclature.

was obtained through m-line spectroscopy for thin organosiloxane films and therefore represents an approximate value for the bulk medium).

Typical results are presented in Figures 1 and 2b−r, which respectively are the temporal plots of peak intensity and effective diameter[37] and corresponding 2-D spatial intensity profiles of the beam acquired at the exit face. The beam self-trapped within 3 s, causing a 4.5-fold decrease in beam diameter from 118 to 26 μm and complementary increase in peak intensity from 0.133 to 0.46 mW·cm^{-2}. At 27 s, the beam narrowed further to 18 μm with an intensity of 1.19 mW·cm^{-2}; the sharp contrast between the initially broad and diffracted beam and its subsequently self-trapped form is evident in Figure 2a,c. The self-trapped beam evolved over the next 388 s, exhibiting complementary oscillations in peak intensity and width (Figure 1). Corresponding spatial profiles showed that the oscillations were due to the onset of high-order optical modes with characteristic spatial intensity profiles (Figure 2b−r). The modes observed during the evolution of the self-trapped beam were identified by comparison with the linearly polarized, high-order optical modes of passive cylindrical waveguides (Figure S2) which were computed using established models.[38−40] Oscillations and individual modes were difficult to resolve (spatially and temporally) after 160 s. However, the beam remained self-trapped and did not revert to its diffracted form; at 415 s, its width was 23 μm (5 times smaller than the diffracted width). At this stage, there was an abrupt and irreversible decrease over the next 6 s in intensity to 0.4 mW·cm^{-2}, which was probably caused by polymerization-induced phase separation in the organosiloxane.[41,42]

2.1.2. Comparison with Theoretical Models. These results do confirm predictions of theoretical models of self-trapping in polymerizable and equivalent one-photon based systems.[5,6,18−22] The theoretical framework summarized here is based on the nonlinear Schrödinger equation (eq 2), which is generally applied to simulate nonlinear light propagation processes.[1,10] The propagation of a Gaussian beam (with diameter $a \gg \lambda/2\pi$, and electric field amplitude ε) according to the paraxial approximation

$$\varepsilon(x, y, 0, t) = \varepsilon_0(-(x^2 + y^2)/a^2) \tag{1}$$

is given by

$$ik_0 n_0 \frac{\partial \varepsilon}{\partial z} + \frac{1}{2}\nabla_t^2 \varepsilon + k_0^2 n_0 \Delta n \varepsilon + \frac{i}{2} k_0 n_0 \alpha \varepsilon = 0 \tag{2}$$

where α is the attenuation coefficient of the medium at wavelength λ corresponding to the free space wavenumber, $k_0 = \omega/c$. The temporal variation of Δn due to polymerization is given by a phenomenological expression

$$\frac{\partial \Delta n}{\partial t} = A(\varepsilon \varepsilon^*)\left(1 - \frac{\Delta n}{\Delta n_s}\right) \tag{3}$$

where A is a material-dependent parameter, and Δn_s is the maximum change of refractive index (at saturation) of the medium.[43] Equation 2 contains terms that describe the counterbalance between natural diffraction (x, y) and self-induced refractive index changes (Δn (x, y, z, t)) of the beam.

Numerical simulations of eqs 1−3 yielded temporal changes in the spatial distribution of refractive index and intensity along the propagation path (z) of the beam. (Calculations of refractive index and intensity based on this same theoretical approach are presented as Supporting Information in Figure S3). From these results, the sequence and temporal evolution of the self-trapping process was proposed, and trends in the modal evolution of the self-induced waveguide were identified.[18−22] Simulations showed that self-trapping begins when the beam induces a gradient-index lens at the entrance face of the medium and self-focuses further along z. From its new focal point, the beam induces a gradient-index channel waveguide along its propagation path. The waveguide traps and guides the beam without diffracting to the exit face. Once self-trapped, the beam continues to increase the refractive index of its waveguide, which concomitantly develops multiple intensity maxima along z. These maxima were attributed to the beating between high-order modes that become excited as the refractive index of the waveguide increases. Because refractive index changes are not uniform along z, the position and number of intensity maxima (and thus the modal composition) vary along the waveguide in a nontrivial way (*vide infra*).

There is excellent agreement between the simulated sequence of self-trapping and the experimental observations presented in Figures 1 and 2. The decrease in width and increase in intensity observed within the first 30 s signifies self-focusing and subsequent self-trapping of the beam in its channel waveguide.[44] An optical micrograph acquired at this point confirmed that a cylindrical waveguide with a diameter of ~40 μm had been

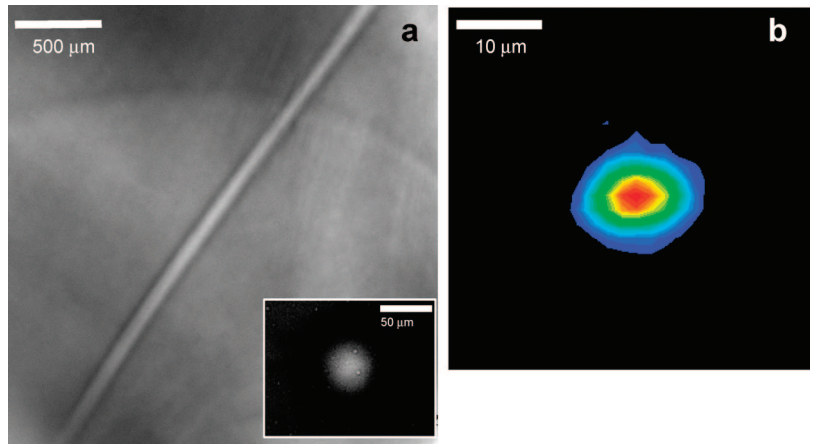

Figure 3. (a) Transmission optical micrograph of the self-written waveguide in the organosiloxane during self-trapping at 1.6×10^{-2} W·cm^{-2}; the inset is a micrograph of its transverse (x, y) cross-section. (b) 2-D intensity profile at the output ($z = 6.0$ mm) of the waveguide guiding light at 532 nm under passive conditions; the output is Gaussian with diameter ($1/e^2$) = 12 μm. Micrographs were acquired through a red filter to prevent polymerization during measurement.

inscribed along z (Figure 3a). Under linear conditions, the waveguide exhibited single-mode guidance (532 nm) with an output-width ($1/e^2$) of 12 μm (Figure 3b). On this basis, the average refractive index change of the waveguide was calculated to be $<7.8 \times 10^{-5}$, which is 2 orders of magnitude smaller than the refractive index change at saturation in the organosiloxane ($\Delta n_s \sim 0.006$).[16,45] The self-trapped beam could therefore continue to raise the refractive index of its own waveguide over time,[46] which in turn led to the sequential excitation of high-order optical modes. Three different high-order modes appeared in sequence and were individually observed at the exit face. Briefly, at 27 s, the fundamental LP_{01} mode (Figure 2c) was succeeded at 35 s by the next-order mode LP_{11} (Figure 2f) followed by the LP_{02} and LP_{21} modes, which appeared at 47 and 134 s, respectively (Figure 2h,o)). Superpositions of high-order modes, including a fourth high-order mode LP_{03} with the LP_{01} mode were also observed (Figure 2e,i,j,n). Comparisons with computed profiles showed that they corresponded to the linearly polarized modes characteristic of cylindrical waveguides such as optical fibers[38−40] (Figure S2, Supporting Information). This is consistent with the cylindrical waveguides induced by self-trapped beams (Figures 3 and 4). In theoretical simulations, the excitation of high-order modes was inferred from the emergence of intensity maxima within the waveguide and corresponding calculations of modal propagation constants.[20] Results from current experiments not only confirm the onset of high-order modes but also enable direct visualization of their spatial intensity profiles in the near-field and *in situ* monitoring of their evolution within the waveguide.

To further confirm that the multiple modes were all excited within the same cylindrical waveguide, optical micrographs were acquired after excitation of LP_{11} and separately at longer times after excitation of LP_{21} (Figures 4b and 4e). Both revealed a single cylindrical waveguide: the waveguide formed after excitation of LP_{11} had an overall diameter of ~72 μm, while that formed after the onset of LP_{21} was 3 times wider with an overall diameter of ~240 μm. Both guided light (532 nm) under passive conditions; guidance was strongly confined to the core with effective output-diameters of 32 and 31 μm, respectively (Figure 4c,f). This is consistent with theoretical simulations, which showed that self-induced waveguides possess a gradient refractive index profile and are thus able to efficiently confine light within their core-regions.[18]

Current results are consistent with numerical simulations of eqs 1−3[20−22] and, separately, Wentzel Kramers Brillouin analysis,[47] which show that the observed sequence of high-order modes propagate within the *same* self-written channel waveguide. The simulations also show that the spatial variations in refractive index occur at smaller rates and are consequently less pronounced than corresponding variations in optical intensity. The self-induced waveguide can therefore host high-order modes with non-Gaussian intensity profiles, even while retaining its cylindrical geometry. In fact, the same property has enabled self-trapping of incoherent white light, which is composed of a randomly and rapidly fluctuating distribution of optical modes, to collectively propagate within a single self-induced waveguide in the organosiloxane.[41,42]

2.1.3. Oscillations of the Self-Trapped Beam. Numerical simulations of eqs 1−3 have predicted that a self-trapped beam in a polymerizable medium would always exhibit oscillatory behavior, due to the evolving modal structure of the self-induced waveguide and the consequent changes in its intensity distribution. (The same changes can be followed in simulations presented in Figure S3 in the Supporting Information). Such theoretical predictions are understandable because the existence of two even modes in a channel waveguide generates intensity maxima positioned at intervals along z with a periodicity (or beat length) of $2\pi/|\beta_1 - \beta_2|$, where β_1 and β_2 are the respective propagation constants of the modes.[47] Such maxima would be periodically positioned in a waveguide with a uniform refractive index profile. The refractive index of a self-induced waveguide, however, varies significantly along z; as a result, both the number of modes and the propagation constant of each individual mode vary along z, which is further confirmed through Wentzel−Kramers−Brillouin analysis.[47] Intensity maxima due to mode-beating are therefore positioned aperiodically along z. In a passive waveguide, such maxima would remain stationary. However, due to the continually changing refractive index profile of the self-induced waveguide, these maxima change position, appearing to translate along z over time. At a constant observation point along z, the apparent translation of maxima would lead to aperiodic oscillations of the overall intensity and width of the self-trapped beam.

Such oscillations of intensity and width were indeed observed in the current study, where the self-trapped beam was monitored over time at a constant point along z (at its exit face). The experimental results gave further insight into the modal evolution of the self-induced waveguide that was not evident in theoretical simulations. For example, theoretical models considered the excitation of only one high-order mode. Furthermore, the

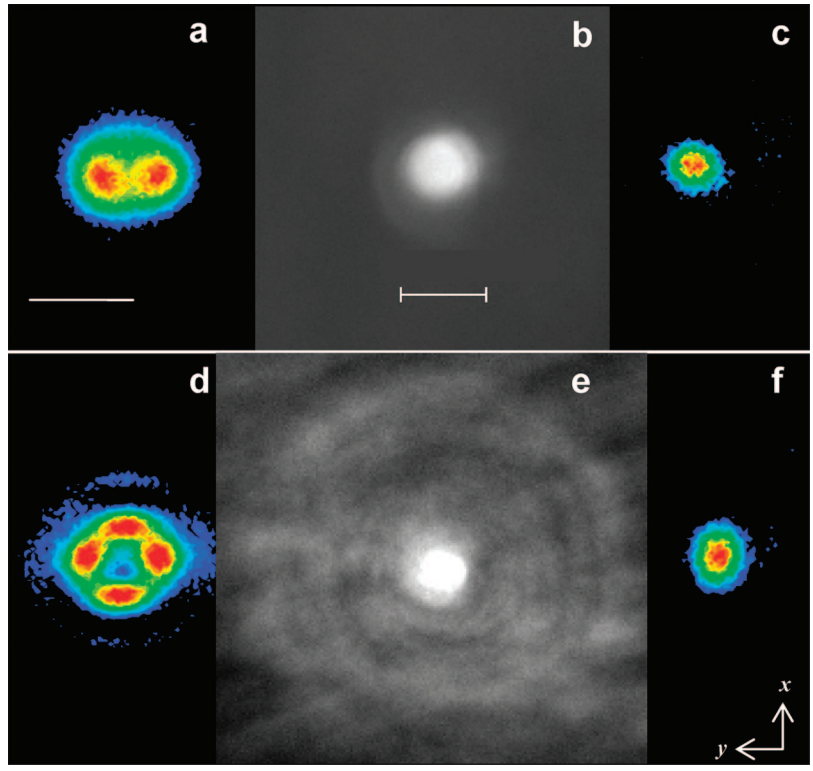

Figure 4. Characterization of self-written waveguides after the onset of higher order modes during self-trapping at 1.6×10^{-2} W·cm^{-2}. (b) Transmission optical micrograph of self-written cylindrical channel waveguide after the onset of (a) LP_{11}. (c) Intensity profile of waveguide output ($z = 6.0$ mm) under passive conditions; output diameter ($1/e^2$) = 32 μm. (e) Cross-sectional micrograph of self-written waveguide after onset of (d) LP_{21}. (f) Intensity profile of waveguide output ($z = 6.0$ mm) under passive conditions; output diameter ($1/e^2$) = 31 μm. Micrographs were acquired through a red filter to prevent polymerization during measurement. The scale bar in (a) also applies to (c), (d) and (f). The scale bar in (b) also applies to (e). Both scale bars = 50 μm.

excitation of the second mode was inferred by its beating with the first and consequent intensity variations along z (see also Figure S4 in the Supporting Information); the spatial intensity profiles corresponding to individual modes were not obtained. In contrast, the experimental results obtained in this study enabled the direct visualization of each of the high-order modes, identifying up to five discrete modes and moreover confirming that they corresponded to optical fiber modes (Figure 2). It was therefore possible, as described below, to identify the exact sequence of optical modes that corresponded to each oscillation of the beam and, in this way, observe the evolution of the modal composition at the waveguide at its output. To our knowledge, there are no previous examples of direct monitoring of the evolution of a cylindrical waveguide from single-mode to multimode guidance.

While oscillations of the self-trapped beam at 1.6×10^{-2} W·cm^{-2} were rapid and irregular (Figure 1), they could be better resolved by carrying out self-trapping at an extremely low intensity, 3.2×10^{-3} W·cm^{-2}, where the rate of refractive index changes (and thus the rate of self-trapping) is significantly lower. As observed in Figure 5a, the crest of an oscillation corresponded to the brightest and narrowest mode, LP_{01}, and the valley corresponded to the highest mode in the sequence. Superposed modes fell between the valleys and crests. Briefly, the first five oscillations showed alternation between modes LP_{01} and LP_{11};[48] once LP_{21} was excited at 67 s, the next four oscillations each consisted of the sequence LP_{01}, LP_{21}, LP_{11}, LP_{01}. Transitions between the pure modes were superpositions of the two: for example, superposition $LP_{11} + LP_{01}$ appeared at 83 s during the transition from LP_{01} to LP_{01}, while $LP_{21} + LP_{11}$ appeared at 115 s between LP_{21} and LP_{11}. A plot of the duration of each oscillation against time showed the theoretically predicted aperiodicity of oscillations and its general increase over time (Figure 5b). The latter can be attributed to the decrease in the rate of refractive index changes, which decreases the rate of change of modal composition and thus the oscillations of the self-trapped beam. Although the sequence of excitation of high-order modes over time corresponds to the sequence supported by optical fibers with increasing indices of refraction, their specific order of appearance, recurrence, and superpositions cannot be fully explained by the existing theoretical models. Further theoretical modeling, which takes into account changes to the intensity distribution in three dimensions is necessary to fully rationalize the specific sequence of appearance of high-order modes.

2.2. Intensity Dependence.

2.2.1. Quantitative Trends in Self-Focusing Time, Self-Trapped Beam Width, and Transmittance. Self-trapping was examined at three intensity regimes that spanned 10 orders of magnitude: low (3.2×10^{-5}, 1.6×10^{-4}, 3.2×10^{-3}, and 8.0×10^{-3}, 1.6×10^{-2} W·cm^{-2}), mid (0.19, 1.6, and 16 W·cm^{-2}), and high (159, 1592, and 12 732 W·cm^{-2}); the beam was Gaussian and linearly polarized with a width ($1/e^2$) of 20 μm at all intensities. Results at each intensity are presented as temporal plots of beam diameter and peak intensity; the most significant changes in the corresponding 2-D spatial intensity profiles are collected as Supporting Information (Figures S4−S7 in). To quantitatively compare self-trapping dynamics in the different intensity regimes, temporal plots were analyzed in terms of 3 selected parameters: (a) self-focusing time, (b) self-trapped beam width, and (c) transmittance ($I_{z=6.0\text{mm}}/I_{z=0.0\text{mm}} \times 100\%$). Each value was averaged over at least three repeat experiments at each intensity; corresponding values of standard deviation are provided (Figure 6).

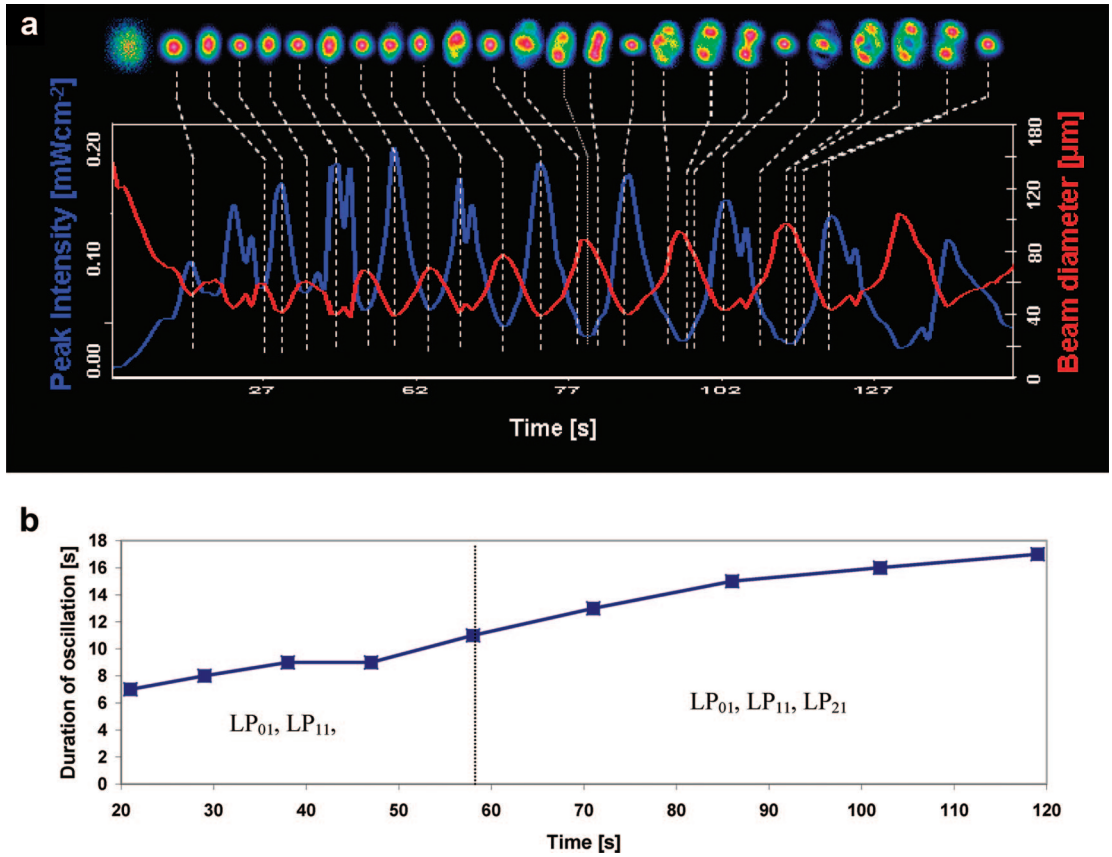

Figure 5. (a) Temporal changes of beam width and peak intensity and corresponding evolution of modal composition at $z = 6.0$ mm during self-trapping at 3.2×10^{-3} W·cm^{-2}. (b) Duration of oscillations over time. The modes identified within each set of oscillations are indicated.

The plot of self-focusing time against initial intensity is approximately parabolic (Figure 6a). In the low intensity regime, self-focusing time varied inversely with intensity, decreasing from 200 ± 90 s to 11 ± 3 s as the initial intensity of the beam was increased from 3.2×10^{-5} W·cm^{-2} to 8.0×10^{-3} W·cm^{-2}. From this minimum, it increased to 21 ± 9 s to 140 ± 30 s in the mid-intensity regime and more significantly to 1300 ± 500 s at 1592 W·cm^{-2} before decreasing to 300 ± 200 s at the greatest intensity of 12 732 W·cm^{-2}.

An explanation for this trend is proposed in Figure 7a, which is a plot of the empirically derived expression for polymerization-induced refractive index change,[5,6]

$$\Delta n(x, y, z, t) = \Delta n_s\left\{1 - \exp\left[-\frac{1}{U_0}\int_0^{t-\tau} |\varepsilon(t)|^2 \mathrm{d}t\right]\right\} \quad (4)$$

where Δn_s is the maximum index change, U_0 is the critical exposure required to initiate polymerization, τ is the monomer radical lifetime, $|\varepsilon(t)|^2$ is the square of the electric field amplitude or intensity (I) of the incident optical field, and t is time.[49]

To self-focus, the beam must induce refractive index changes in the form of its own Gaussian profile at the entrance face of the medium. Figure 7b depicts how such lenses are induced at intensities in the low, mid, and high-intensity regimes. The strongest lens would possess the steepest gradient, with the maximum possible refractive index (Δn_s) localized to the axial region with a radially symmetric decay from this point. In the low-intensity regime, long times ($t \gg \tau$) are necessary to achieve Δn_s even at the (most intense) axial region of the beam. Because I and t vary inversely (until Δn_s is reached), the time required to induce a lens with the strongest gradient also varies inversely with intensity within the low-intensity regime, leading in turn to the inverse relationship between self-focusing time and intensity (Figure 6a).

The trend is reversed in the mid and high-intensity regimes, where increasingly larger cross-sections of the beam *simultaneously* achieve saturation; Δn_s is therefore delocalized over a larger area. Lenses are wider and weaker with smaller numerical apertures that collect and focus light less efficiently;[50] self-focusing consequently requires increasingly longer times.

The variation of the self-trapped beam-width in the different intensity regimes is consistent with the above-proposed mechanism (Figure 6b). Strong lenses induced in the low-intensity regime confine light most efficiently; the self-trapped beam-width thus decreased from 31 ± 4 μm to only 12 ± 3 μm. The trend was reversed in the mid-intensity regimes, where weaker lenses lead to a corresponding increase in self-trapped beam-width, which ranged from 18.0 ± 0.6 μm to 25 ± 3 μm. In the high intensity regime, the width was 70 ± 40 μm and effectively no change in width was observed at the greatest intensity of 12 732 W·cm^{-2}. The anomalous increase in width to 200 ± 50 μm at 159 W·cm^{-2} is due to beam filamentation at this intensity (*vide infra*).

Transmittance of light is most efficient in waveguides with gradient refractive index relative to uniform (step) index profiles.[40] Accordingly, the measured transmittance of self-induced waveguides was greatest during self-trapping in the low intensity regime (Figure 6c). In fact, the maximum value of transmittance was achieved during self-trapping at 8.0×10^{-3} W·cm^{-2}; this is the intensity at which the most rapid self-focusing and smallest self-trapped diameter were observed.

Measurements of these parameters showed a high degree of reproducibility of self-trapping experiments in the low and mid-

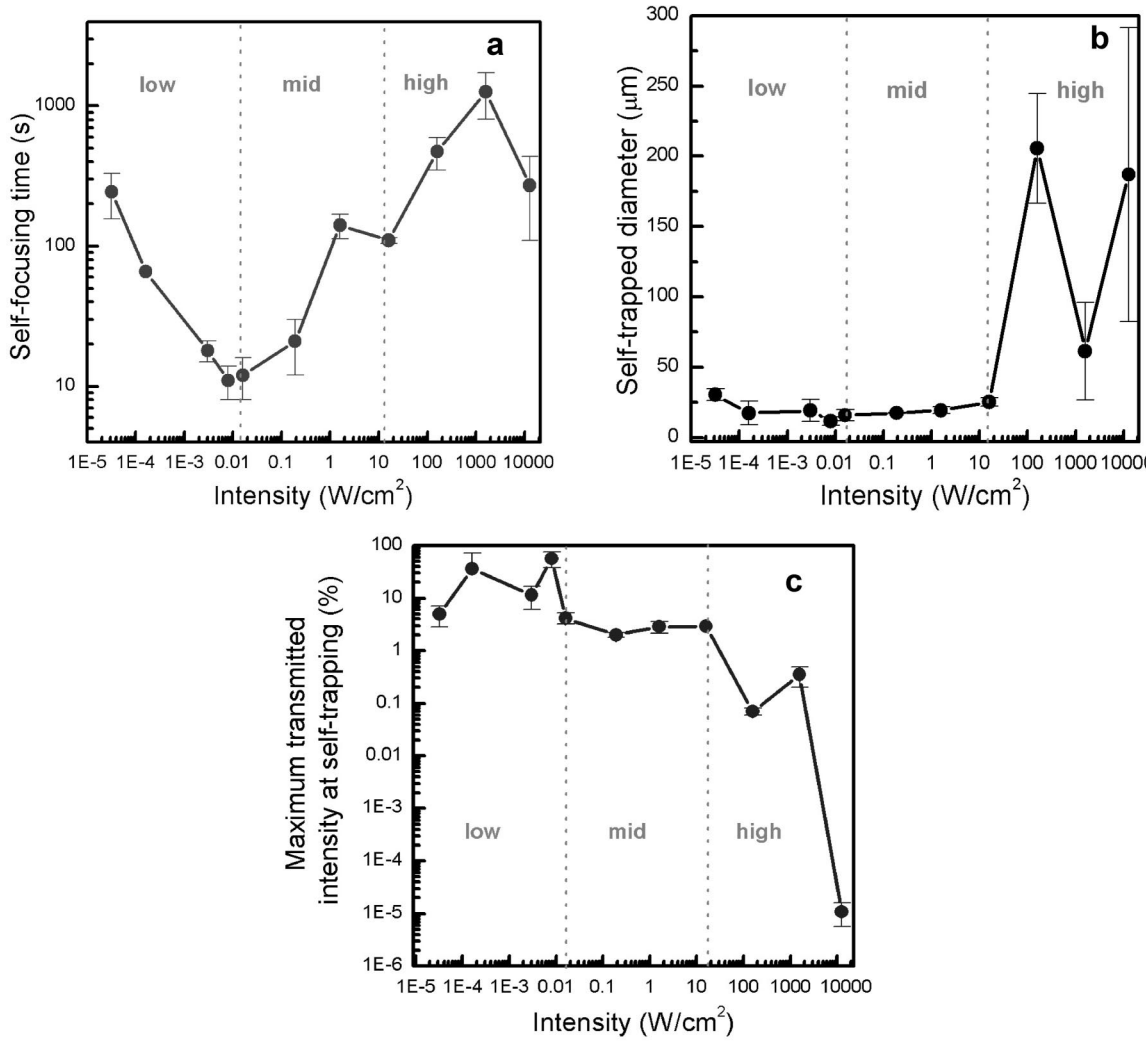

Figure 6. Plots of the initial average intensity of the beam versus self-trapping parameters: (a) self-focusing time, (b) diameter of self-trapped beam, and (c) transmittance (%) during self-trapping. The low, mid, and high-intensity regimes are marked with dotted lines. Error bar = 1 × σ.

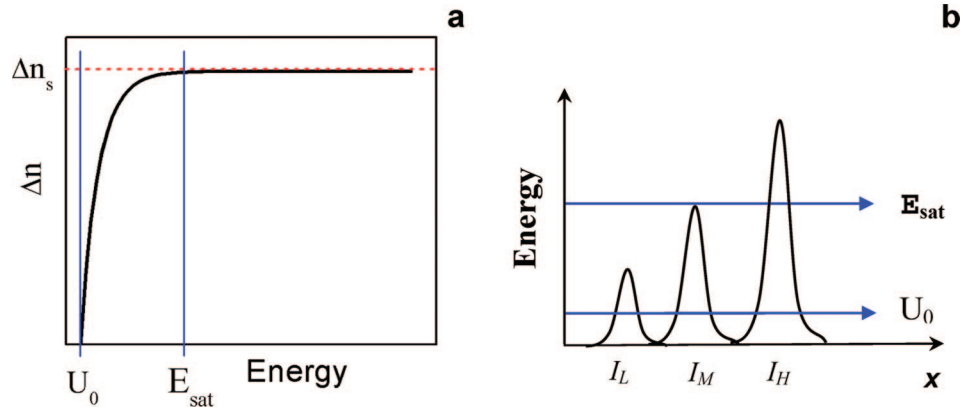

Figure 7. Plots of eq 4: (a) Refractive index change as a function of energy, where U_0 = critical exposure required for photoinitiation and E_{sat} = energy required to achieve Δn_s = refractive index change at saturation. (b) 1-D spatial profiles (along x) of the Gaussian beam and corresponding optical energy after 1 s of exposure. Relative positions of E_{sat} and U_0 are indicated.

intensity regimes. Standard deviations of parameters were, in general, significantly greater in the high-intensity regime. Because free-radical polymerization is an exothermic process, increased reaction rates at these extremely high intensities may lead to convection currents and inhomogeneities in the medium that cause scatter and, in this way, contribute to variations between experiments.

2.2.2. Spatial Beam Profiles: High-Order Modes, Spatial Diffraction Rings, and Filamentation. 2-D spatial intensity profiles acquired during self-trapping at different intensities showed striking differences in the behavior of beams within each intensity regime. 2-D profiles are collected in Figures S5−S7 in the Supporting Information; representative profiles are presented in Figure 8. In the low-intensity regime, self-

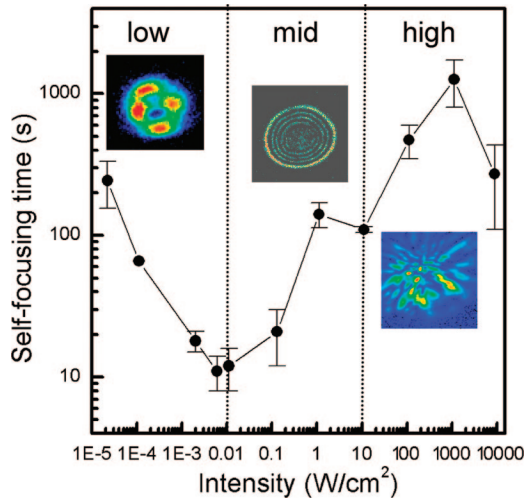

Figure 8. Representation of the three different forms of nonlinear light propagation in the photopolymerizable organosiloxane in the three intensity regimes. The low-intensity regime is characterized by the modal evolution of the self-trapped beam, while self-diffraction rings and beam filamentation occur in the mid and high-intensity regimes, respectively. Complete spatial intensity profiles of the beam at all intensities are provided as Figures S5−S7 in the Supporting Information.

trapping at all intensities followed the theoretically predicted sequence of self-focusing, waveguide formation and excitation of high-order modes. The principal difference was the absolute number of high-order modes excited in the waveguide. Because the rate of refractive index change decreases with decreasing intensity (Equation [4]), waveguides induced at smaller intensities have smaller values of refractive index change and can therefore support fewer modes.[40] For example, only three modes (LP_{01}, LP_{11} and LP_{21}) were identified at the three lowest intensities (3.2×10^{-5}, 1.6×10^{-4} and 3.2×10^{-3} Wcm^{-2}) whereas five modes (LP_{01}, LP_{11}, LP_{21}, LP_{02} and LP_{03}) were evident during self-trapping at 8.0×10^{-3} and 1.6×10^{-2} Wcm^{-2}.

The resolution of high-order modes was not possible during self-trapping in the mid-intensity regime. Here, refractive index changes occurred at greater rates and the entire self-trapping process was completed within a significantly reduced period of time. (For example, the average duration of self-trapping[51] was 703 s at the low intensity of 1.6×10^{-2} $W \cdot cm^{-2}$, whereas it was only 184 s at the mid intensity of 16 $W \cdot cm^{-2}$). As a result, the self-induced waveguide rapidly achieves saturation and is rendered multimoded at early times, as observed at the output during self-trapping at 0.19 $W \cdot cm^{-2}$ (Figure S6 in the Supporting Information). An entirely different phenomenon was also observed in the mid-intensity regime at 1.6 $W \cdot cm^{-2}$. Here, spatial profiles showed the emergence of an increasing number of concentric rings at the output (Figure S6 in the Supporting Information). Such patterns have previously been observed during the nonlinear propagation of Gaussian beams in photorefractive crystals[52] and Kerr media.[53,54] The rings, which have been treated either as self-diffracting effects due to spatial self-phase modulation[53,54] or as dispersive (rather than dissipative) spatial shock waves,[52] occur under similar conditions that give rise to self-trapping and will be further examined in future studies.

In the high-intensity regime, the beam predominantly underwent filamentation, fragmenting into multiple segments that self-trapped individually. Because lenses induced in this regime are extremely weak, the beam remains broad and unfocused. Filamentation therefore occurs through a mechanism similar to modulation instability of broad, uniform beams,[55,56] where random noise (minor variations in refractive index or intensity) imposed on the beam become amplified under nonlinear conditions and ultimately cause disintegration of the beam into individual self-trapped filaments.

3. Summary and Outlook

This experimental study provides a comprehensive overview of the nonlinear propagation of a continuous-wave Gaussian laser beam in a medium undergoing photopolymerization. These results confirmed and provided new insight into key predictions of theoretical models developed in the past decade, such as the excitation of high-order optical modes of the self-trapped beam and concomitant self-inducement of a multimode waveguide. Most significantly, these experiments provided an extremely rare opportunity to directly observe the excitation of individual higher order modes during the evolution of a cylindrical waveguide from single-mode to multimode guidance. Trends in the oscillatory behavior of the modes during this process were consistent with those predicted by theory. Further modeling, specifically calculations of the 3-D distribution of intensity and refractive index during self-trapping, is necessary to fully explain the exact sequence of modes observed and is the subject of our current investigations. Such an understanding would also be greatly valuable in characterizing the complex modal composition of multimode optical fibers, where it is not possible to individually resolve higher order modes.[40] Quantitative analyses of self-trapping at a broad range of intensities revealed the significance of the gradient of photoinduced refractive index changes, showing that self-trapping was most efficient in the low-intensity regime where the steepest gradients are induced. A new form of nonlinear propagation in photopolymerizable media, spatial diffraction rings, was observed in the mid-intensity regime, whereas beam filamentation dominated at extremely high intensities. Future work will also examine the latter phenomena.

Acknowledgment. Funding from NSERC, CFI, and McMaster University and donation of the photoinitiator, IRGACURE-784 by CIBA-Geigy, Inc., is gratefully acknowledged. We thank Jonathan Lannan for developing initial beam propagation simulations and Prof. Andrew Knights (Department of Engineering Physics, McMaster) for useful suggestions and comments.

Supporting Information Available: Experimental methods, beam propagation simulations of optical fiber modes and optical self-trapping, and temporal and spatial characterization of nonlinear light propagation in all intensity regimes. This material is available free of charge via the Internet at http://pubs.acs.org.

References and Notes

(1) Trillo, S., Torruellas, W., Eds. *Spatial Solitons*; Springer: New York, 2001; pp 19−33.
(2) Chiao, R. Y.; Garmire, E.; Townes, C. H. *Phys. Rev. Lett.* **1964**, *13*, 479–482.
(3) Segev, M. *Opt. Quantum Electron.* **1998**, *30*, 503–533.
(4) Monro, T. M.; Moss, D.; Bazylenko, M.; Matijn de Sterke, C.; Poladian, L. *Phys. Rev. Lett.* **1998**, *80*, 4072–4075.
(5) Kewitsch, A.; Yariv, A. *Opt. Lett.* **1996**, *21*, 24–26.
(6) Kewitsch, A.; Yariv, A. *Appl. Phys. Lett.* **1996**, *68*, 455–457.
(7) Shoji, S.; Kawata, S.; Sukhorukov, A. A.; Kivshar, Y. S. *Opt. Lett.* **2002**, *27*, 185–187.
(8) Sukhorukov, A. A.; Shoji, S.; Kivshar, Y. S.; Kawata, S. *J. Nonlinear Opt. Phys. Mater.* **2002**, *11*, 391–407.
(9) Dorkenoo, K.; Cregut, O.; Mager, L.; Gillot, F.; Carre, C.; Fort, A. *Opt. Lett.* **2002**, *27*, 1782–1784.

(10) (a) Stegeman, G. I.; Segev, M. *Science* **1999**, *286*, 1518–1523. (b) Segev, M.; Stegeman, G. I. *Phys. Today* **1998**, *51*, 42–48.

(11) Chen, Z.; Mitchell, M.; Segev, M.; Coskun, T. H.; Christodoulides, D. N. *Science* **1998**, *280* (5365), 889–892.

(12) Christodoulides, D. N.; Coskun, T. H.; Mitchell, M.; Chen, Z.; Segev, M. *Phys. Rev. Lett.* **1998**, *80*, 5113–5116.

(13) Cohen, O.; Buljan, H.; Schwartz, T.; Fleischer, J. W.; Segev, M. *Phys. Rev. E: Stat., Nonlinear, Soft Matter Phys.* **2006**, *73(1−2)*, 015601/1–015601/4.

(14) Christodoulides, D. N.; Coskun, T. H.; Joseph, R. I. *Opt. Lett.* **1997**, *22*, 1080–1082.

(15) Mitchell, M.; Segev, M. *Nature (London)* **1997**, *387*, 880–883.

(16) Saravanamuttu, K.; Du, X. M.; Najafi, S. I.; Andrews, M. P. *Can. J. Chem.* **1998**, *76*, 1717–1729.

(17) Decker, C. *Polym. Int.* **1998**, *45*, 133–141.

(18) Monro, T. M.; De Sterke, C. M.; Poladian, L. *J. Mod. Opt.* **2001**, *48*, 191–238.

(19) Monro, T. M.; Poladian, L.; De Sterke, C. M. *Phys. Rev. E: Stat. Phys., Plasmas, Fluids, Relat. Interdiscip. Top.* **1998**, *57*, 1104–1113.

(20) Monro, T. M.; Martijn de Sterke, C.; Poladian, L. *J. Opt. Soc. Am. B* **1996**, *13*, 2824–2832.

(21) Monro, T. M.; Martijn de Sterke, C.; Poladian, L. *Opt. Commun.* **1995**, *119*, 523–526.

(22) Monro, T. M.; Miller, P. D.; Poladian, L.; Martijn de Sterke, C. *Opt. Lett.* **1998**, *23*, 268–270.

(23) Frisken, S. J. *Opt. Lett.* **1993**, *18*, 1035–1037.

(24) Shoji, S.; Kawata, S. *Appl. Phys. Lett.* **1999**, *75*, 737–739.

(25) Dorkenoo, K. D.; Gillot, F.; Cregut, O.; Sonnefraud, Y.; Fort, A.; Leblond, H. *Phys. Rev. Lett.* **2004**, *93*, 143905-1–143905-4.

(26) Saravanamuttu, K.; Andrews, M. P. *Opt. Lett.* **2002**, *27*, 1342–1344.

(27) Sugihara, O.; Tsuchie, H.; Endo, H.; Okamoto, N.; Yamashita, T.; Kagami, M.; Kaino, T. *IEEE Photonics Technol. Lett.* **2004**, *16*, 804–806.

(28) Yamashita, K.; Hashimoto, T.; Oe, K.; Mune, K.; Naitou, R.; Mochizuki, A. *IEEE Photonics Technol. Lett.* **2004**, *16*, 801–803.

(29) Kagami, M.; Yamashita, T.; Ito, H. *Appl. Phys. Lett.* **2001**, *79*, 1079–1081.

(30) Yamashita, T.; Kagami, M.; Ito, H. *J. Lightwave Technol.* **2002**, *20*, 1556–1562.

(31) Yonemura, M.; Kawasaki, A.; Kato, S.; Kagami, M.; Inui, Y. *Opt. Lett.* **2005**, *30*, 2206–2208.

(32) Ozawa, H.; Obata, Y.; Mimura, Y.; Mikami, O.; Shioda, T. *IEEE Photonics Technol. Lett.* **2006**, *18*, 880–882.

(33) Bachelot, R.; Ecoofet, C.; Deloeil, D.; Royer, P.; Lougnot, D.-J. *Appl. Opt.* **2001**, *40*, 5860–5871.

(34) (a) Obata, Y.; Kanda, M.; Mikami, O. *IEEE Photonics Technol. Lett.* **2006**, *18*, 1308–1310. (b) Streppel, U.; Dannberg, P.; Wachter, C.; Brauer, A.; Kowarschik, R. *Appl. Opt.* **2003**, *42*, 3570–3579.

(35) (a) Jeong, K. H.; Kim, J.; Lee, L. P. *Science* **2006**, *312*, 557–561. (b) Kim, J. Y.; Jeong, K. H.; Lee, L. P. *Opt. Lett.* **2005**, *30*, 5–7.

(36) Saravanamuttu, K.; Blanford, C. F.; Sharp, D. N.; Dedman, E. R.; Turberfield, A. J.; Denning, R. G. *Chem. Mater.* **2003**, *15*, 2301–2304.

(37) The effective beam diameter is the diameter of a circle with an area equal to the area of all the pixels with intensity above 13.5% of the measured beam peak intensity in the CCD camera.

(38) Okoshi, T. *Optical Fibers*; Academic Press, Inc.: New York, 1982.

(39) Belanger, P-A. *Optical Fiber Theory: A Supplement to Applied Electromagnetism*; World Scientific Publishing Co., Pte. Ltd.: River Edge, NJ, 1993; Chapter 5, pp 144−182.

(40) Buck, J. A. *Fundamentals of Optical Fibers*; Wiley and Sons, Inc.: New York, 2004.

(41) Zhang, J.; Kasala, K.; Rewari, A.; Saravanamuttu, K. *J. Am. Chem. Soc.* **2006**, *128*, 406–407.

(42) Zhang, J.; Saravanamuttu, K. *J. Am. Chem. Soc.* **2006**, *128*, 14913–14923.

(43) Equation 3 reflects the kinetics of free-radical polymerization, where the propagation rate is proportional to intensity ($\varepsilon\varepsilon^*$) and decays exponentially as the concentration of polymerizable monomers decreases (as $\Delta n/\Delta n_s \rightarrow 1$).

(44) In a physical system, a Gaussian beam can form a lens only if refractive index changes are proportional to intensity and spatially localized (with resolution $< \lambda$). Under these conditions, the beam induces an index gradient in the form of its own non-uniform profile, with maximum Δn at the axial (most intense) region and a circularly symmetric decay from this point. Whereas most polymerization reaction rates (thus Δn) are intensity-dependent, rapid diffusion of free-radical propagators in free monomer-based systems causes blurring of Δn, especially at large intensities. Δn in the organosiloxane by contrast has excellent spatial resolution of $\sim$0.15 μm,[36] enabling the 20 μm-wide beam employed in this study to induce a lens at $z = 0.00$ mm.

(45) Δn of the single-mode waveguide can be approximated using the expression that describes monomode operation $[(2\pi a/\lambda)(n_1^2 - n_2^2)^{1/2} < \approx 3.58]$ of a waveguide with a gradient refractive index profile,[38−40] where $a = 20$ μm (radius of self-written waveguide, Figure 3).

(46) That the self-trapped beam *evolves* in this way is in itself different from the behavior of 2-D self-trapped beams in photorefractive media. Δn_s in photorefractive crystals is small ($\sim 10^{-4}$),1 and the system generally saturates upon self-trapping; because no further change in refractive index is possible, the self-trapped beam remains stable in intensity and width.

(47) Monro, T. M.; Martijn de Sterke, C.; Poladian, L. *J. Opt. Soc. Am. B* **1999**, *16*, 1680–1685.

(48) At early stages, the intensity profile of LP_{11} was not well-resolved (probably due to insufficient Δn at early times). However, the anisotropic elliptical shape of the beam was strongly characteristic of the LP_{11} mode.

(49) Equation 4 is equivalent to eq 3.

(50) Numerical aperture of a gradient index lens is given by $\sin\theta = (n_a^2 - n_o^2)^{1/2}$, where θ is the maximum acceptance angle of the lens, n_a is its maximum refractive index at the axis, and n_o is the refractive index at its edge.

(51) The duration of self-trapping was defined as the time over which the beam remained significantly narrower (at least $> \sim$1.5 fold) and more intense than its diffracted form.

(52) Wan, W; Jia, S.; Fleischer, J. W. *Nat. Phys.* **2007**, *3*, 46–51.

(53) Trejo-Durán, M.; Andrade-Lucio, J. A.; Martínez-Richa, A.; Vera-Graziano, R.; Castaño, V. M. *Appl. Phys. Lett.* **2007**, *90*, 091112–091113.

(54) Nascimento, C. M.; Alencar, M. A. R. C.; Chávez-Cerda, S.; da Silva, M. G. A.; Meneghetti, M. R.; Hickmann, J. M. *J. Opt. A: Pure Appl. Opt.* **2006**, *8*, 947–951.

(55) Burgess, I. B.; Shimmell, W. E.; Saravanamuttu, K. *J. Am. Chem. Soc.* **2007**, *129*, 4738–4746.

(56) Streppel, U.; Dannberg, P.; Wächter, C.; Bräuer, A.; Kowarschik, R. *Appl. Opt.* **2003**, *42*, 3570–3579.

JP801342N